Quaternary Geochronology 68 (2022) 101253

Contents lists available at ScienceDirect

Quaternary Geochronology

journal homepage: www.elsevier.com/locate/quageo

Luminescence dating of mass-transport sediment using rock-surface burial methods: A test case from the Baksan valley in the Caucasus Mountains

A.C. Cunningham [a,b,*], D. Khashchevskaya [c], D. Semikolennykh [c,d], R. Kurbanov [c,d], A. S. Murray [a]

[a] Department of Geoscience, Aarhus University, Risø Campus, DK-4000, Roskilde, Denmark
[b] DTU Physics, Technical University of Denmark, Risø Campus, DK-4000, Roskilde, Denmark
[c] Moscow State University, Leninskiye Gory 1, 119991, Moscow, Russia
[d] Russian Academy of Sciences, Institute of Geography, Staromonetny pereulok 29, Moscow, Russia

A B S T R A C T

Mass-transport sediments are generally difficult to date directly by existing methods. Conventional luminescence dating of sand is unsuitable because the short transport distances provide little opportunity for bleaching. However, larger clasts are often exposed to sunlight for prolonged periods before becoming entrained in mass-movements, and these clasts have the potential to be used for rock-surface luminescence dating. Mass-transport is a major component of landscape change in mountain regions; in the Baksan valley, Caucasus Mountains, high uplift rates and high precipitation create a rapidly eroding landscape where preservation of sediments is poor. The area is particularly prone to destructive debris flows, because of the large quantity of detrital material in the catchments. The debris-flow and hillslope sediment the Baksan valley are used here to test the applicability of rock-surface burial dating to mass-transport sediment. We find that colluvial clasts show a high degree of bleaching and give reproducible ages, with a large colluvial deposit dated to the early–mid Holocene. The bleaching of debris flow clasts is more variable – we suppose due to the more complex transport history of the clasts, with opportunities for lengthy storage in moraines or colluvium. Overall, the results are encouraging, and suggest that rock-surface methods can provide a useful approach to mass-transport dating in mountainous regions. However, improved targeting of samples and measurement efficiency is desirable for widespread application.

1. Introduction

Understanding the timing and evolution of mass-transport events is both important and challenging. These events include rockfalls, landslides, debris flows, hillslope scree and colluvium; they cover some of the major processes of slope erosion and landscape evolution, and provide important mechanisms for mass wasting in high relief catchments. All are heavily influenced by rainfall, prevailing moisture and temperature, and so their recurrence and magnitude may change over time in response to climatic changes. Mass movements pose a serious hazard to human population and infrastructure in mountainous areas, and understanding the timing of processes that lead to slope failure is essential to the development of site-specific risk assessments. Unfortunately mass-transport sediments are very difficult to date directly, and chronologies are usually based on indirect methods, e.g. luminescence or radiocarbon dating of bracketing sediment or entrained organic material. Conventional luminescence dating of sand grains is generally unsuitable, because the short duration of sediment transport makes sufficient resetting or bleaching of the latent luminescence signal unlikely (see Fuchs, 2019). Similarly, cosmogenic nuclide dating suffers from inheritance of pre-event cosmogenic nuclides and large uncertainties.

Sunlight bleaching of rock surfaces causes the latent luminescence signals of surficial mineral grains to be depleted. These latent signals increase after burial through the absorption of energy from ionizing radiation, and so the burial date of the rock surface can be estimated using Optically Stimulated Luminescence (OSL) dating procedures. This approach has been applied successfully in several archaeological contexts, where the surfaces of stone structures provide a suitable rock surface as dosimeter (e.g. Greilich et al., 2005; Vafiadou et al., 2007; al Khasawneh et al., 2019); the related method of thermoluminescence dating has previously been applied to marble structures (see King et al., 2019). As with other applications of luminescence dating, the question of bleaching (also called resetting or zeroing) is of paramount importance. Routine application of the method requires confidence that the rock surface received enough light to reset the OSL signal before burial, but this is not evident from the measurement of surface material. However, in prolonged exposure to daylight, the latent OSL signals in rock can be bleached to a depth of several millimetres or more. The

* Corresponding author. Department of Geoscience, Aarhus University, Risø Campus, DK4000, Roskilde, Denmark.
E-mail address: alastair.cunningham@rhul.ac.uk (A.C. Cunningham).

https://doi.org/10.1016/j.quageo.2022.101253
Received 21 April 2021; Received in revised form 18 January 2022; Accepted 19 January 2022
Available online 24 January 2022

change in signal with depth is dependent on the total amount of light exposure, among other rock-specific parameters, and can be analysed using the theoretical framework provided by Sohbati et al. (2011, 2012) and Freiesleben et al. (2015). Within this framework, OSL depth profiles can be investigated for evidence of sufficient bleaching, providing an internal check on the validity of rock-surface burial ages. These findings have given renewed impetus to the investigation rock-surface luminescence as a means of dating natural sediment, and of most interest are those clast-rich sediments that are difficult to date using existing methods. Recent work has shown encouraging results for beach cobbles (Simms et al., 2011; Souza et al., 2021), glacial moraines (Rades et al., 2018), and for fluvial and glacio-fluvial clasts (Liu et al., 2019; Jenkins et al., 2018). Mass-transport deposits are also potentially amenable to rock-surface burial dating because the larger embedded clasts (cobbles, boulders) were often part of the hillslope surface before the most recent transport event, and so had the opportunity to be light-exposed for a considerable period before final emplacement. In upland catchments, the disintegration of bedrock (e.g. by freeze-thaw action) may also give clasts with at least one face with prolonged exposure to daylight.

We chose the Baksan valley in the Greater Caucasus to test the application of rock-surface luminescence dating to mass-transport sediment. The central Caucasus is particularly prone to debris flows, due to a very high uplift rate, high precipitation, and accumulated glacial detritus. The lithology of the mainly granite catchments is amenable to measurement using the luminescence signal from feldspar, and the relatively light colour of the granite is known from experience to be associated with good light penetration. Nevertheless, the degree to which clasts incorporated in mass-transport deposits were bleached before burial remains unknown until returned to the laboratory for measurement. Here, we adapt the typical measurement procedures so that burial ages may be estimated for sites with very uncertain bleaching conditions. More specifically, we aim:

- To measure as many clasts, and faces of clasts, as possible, to increase the probability of finding cores with good bleaching profiles.
- To derive an estimate of burial age for clasts where pre-burial bleaching is incomplete (i.e. providing an imprecise, or maximum, burial age, rather than rejecting the clast).
- To reduce the amount of sample material required for estimation of the clast burial age.

This strategy requires innovations in the measurement procedures and profile fitting routines, and also in dose rate measurement procedures. Because resources are finite, the measurement of a greater number of clasts and cores requires a reduction in the number of measurements per core. Hence, the procedures used here are expected to reduce the precision of the burial age estimates for individual clasts, while increasing the overall dating accuracy for the sites in question.

2. Methods

2.1. Site description

Sampling took place in four locations in the upper reach of the Baksan river between Elbus and Tyrnauz, in Kabardino-Balkaria, Russian Federation (Fig. 1). The Baksan river rises on the southern slopes of the dormant volcano Mt Elbrus, and the river valley is one of the main drainage channels of the central Caucasus. During Pleistocene glaciations it is likely to have held a major outlet glacier. Modelling studies suggest a maximum late Pleistocene glacial length of ~70 km (Gobejishvili et al., 2011); however, preservation of moraines in the Caucasus is generally poor, due to the high rates of erosion, and there are very few radiometric dates, or palaeoclimate datasets, from the region (Solomina et al., 2015).

The tributaries of the Baksan contain 150 modern glaciers, descending to 2700–3100 m altitude (Tarbeeva, 2008). Moraines, along with slope and proluvial deposits, provide abundant source material for the large and frequent debris flows in the region. There are 15 large debris basins in the main valley between Elbrus and Tyrnauz, with prominent debris cones where the tributaries enter the Baksan valley. Debris flows are a regular occurrence in recent times, and may be becoming more frequent due to glacial retreat (Seinova et al., 2007). The main towns and settlements, including Tyrnyauz, Elbus, and the Neutrino observatory, have been built on debris cones, many of which are known to be still active. Devastating debris flows have caused loss of life, property and infrastructure every few years; seven particularly destructive debris flows hit Tyrnauz between 1937 and 2000 (Seinova et al., 2003).

The chosen sampling locations cover a variety of debris and mass-movement deposits. Cobble-sized clasts from each site were collected during the day, with any exposed sides spray painted so that they could be excluded from later analysis. On site, cobbles were swiftly wrapped in metal foil and black plastic. The duration of daylight exposure during sampling is negligible compared to the many months of exposure

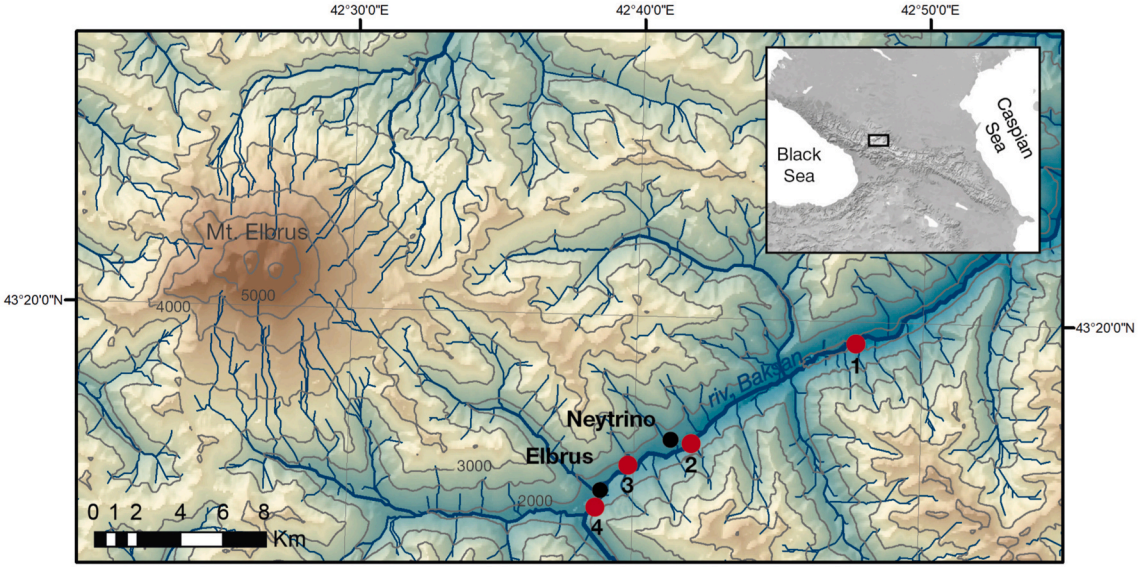

Fig. 1. Elevation map of the upper Baksan valley, situated near Mt Elbrus in the Greater Caucasus range. Samplings sites 1–4 are indicated.

required to bleach the feldspar IRSL signal even in surface grains.

Site 1 (Fig. 2a) is a prominent river-cut exposure of a very large colluvial deposit below a south-facing slope. The exposure is > 1 km in length and ~100 m high at the centre. The deposit is composed of cobble-sized clasts of granite, with very little finer material. A limited degree of bedding is evident, with coalesced debris cones centred under small gullies in the overlying slope. The surface of the deposit has a thin layer of sparse vegetation. Active, uncovered lobes of cobbles can be seen in some places. The lower parts of the section are covered by slump or scree. We sampled three locations above the scree (T4, T5, T6) in stratigraphic order. In addition, at location T8 several buried clasts were taken from near the surface, at a depth of ~10 cm. Location T7 lies at the base of the section, but is not in its original position. Scour marks on the section above indicate that the unit is part of a large landslip, presumably formed after the river undercut the section. Within the unit the bedding is intact; thus the ages derived from this location are unaffected by the recent landslip, but the original position of the unit is uncertain.

Site 2 is a recent road-cut section through a prominent feature of uncertain origin known as Tyubele Swell. The hill is between 500 and 900 m long, up to 170 m high. The sediment has a complex structure, with a lower unit that resembles a section through a debris cone of cobble-sized clasts, overlain by a less structured sediment including large boulders. The feature has been interpreted as either a mixture of moraine and debris flow from the AdyrSu valley to the south or the result of a landslide falling onto a Pleistocene glacier in the Baksan valley (Koronovsky and Milanovsky, 1960); or the result of seismic landslide (Bashenina et al., 1974) or collapsed debris flow (Shcherbakova, 1973).

Site 3 is a surface deposit from an active debris flow between the settlements of Elbrus and Neutrino, at the mouth of the Sagayevsky stream joining the Baksan from the south. The site is the most active debris flow in the valley, with new material being deposited every few years, derived from a large accumulation of nivation products in the north-facing Sagayevsky valley (Tarbeeva, 2008). A significant debris flow had occurred only a few weeks before sampling, and the road remained partially covered. Protruding surface cobbles were still covered with a thin layer of finer sediment (Fig. 2d and e), suggesting that there had been no significant rainfall since the event.

Site 4 is a rivercut section of a small debris cone, on the outskirts of Elbrus town. The debris cone lies at the base of a short, steep, north-facing valley, near the confluence of the Adylsu and the Baksan rivers. The section is ~40 m wide, ~8 m high. The debris material is predominantly cobbles in a clast-supported matrix, with intercalated beds of gravel and finer sediment. The debris units are well stratified, dipping away from the apex (see Fig. 9) An active debris channel is also present.

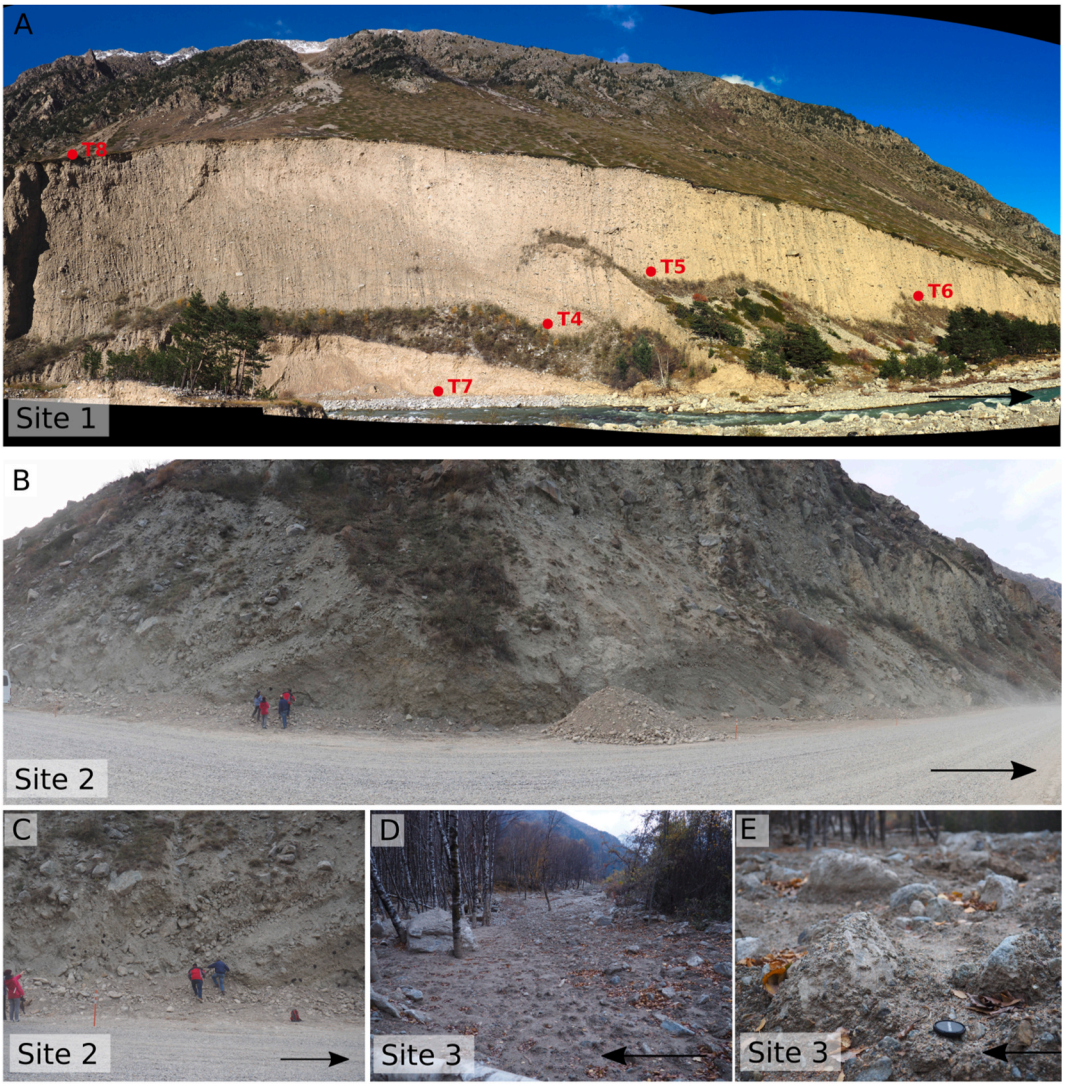

Fig. 2. Photographs of Sites 1–3. (a) Composite photograph of Site 1, a river cutting of a colluvial deposit. (b) and (c): Roadcut section of the Tubelle swell, Site 2. Samples were collected from stratified debris units where the people are standing. (d) and (e): Surface sediment of a recently active debris flow (Site 3). Arrows indicate flow direction of the Baksan River.

Underlying the debris cone is a bed of well-rounded fluvial cobbles.

2.2. Equivalent dose

2.2.1. Sample preparation and instrumentation

Cores (10 mm Ø) were extracted from cobble-sized clasts using a water-cooled, diamond-tipped coring drill, under subdued dark-room lighting. Cores were drilled from each – typically two – of the major faces of the clasts, excluding the faces known to have been exposed to daylight before or during sampling. Cores were then sliced transversely using a water-cooled wafering saw with increments of 1.5 mm; the resulting slices have a thickness of ~1.2 mm. Additional cores were drilled for each clast to provide material for dose rate analysis.

Luminescence measurements were made on one of several Risø luminescence readers, Model TL-DA15, incorporating a $^{90}Sr/^{90}Y$ beta source. The readers are equipped with infra-red (850 ± 30 nm) LEDs, and luminescence was detected through combined Schott BG-39 and Corning 7–59 glass filters, transmitting in blue–violet wavelengths. For measurement, in most cases rock slices were placed directly on the carousel, but for some cores, the slices were broken up and chips placed in steel cups on the carousel. The instrumental beta dose rate was calibrated using gamma-irradiated quartzite slices (Hansen et al., 2018) in the appropriate geometry.

2.2.2. Measurement protocol

Measurements followed a post-IR SAR protocol (Buylært et al., 2012) with a preheat of 250 °C for 100 s, IR stimulation at 50 °C for 200 s, followed by the second IR stimulation at 225 °C for 200 s. The background-subtracted signals were used to construct the dose-response curves, fitted with a single saturating exponential function. The reliability of the measurement protocol was checked using dose-recovery tests, including a sensitivity test of the measurement parameters (Fig. 3). For this, unmeasured slices from two cores were bleached in a solar simulator for 24 h, then given a 60 Gy dose using the beta source. The recovered doses are plotted against preheat temperature (Fig. 3a) and test-dose size (Fig. 3b). For the chosen conditions of 250 °C preheat and 12 Gy test dose, the recovered doses lie in the range of 0.81–0.98 for IR_{50} measurements, and 1.07–1.20 for $pIRIR_{225}$ measurements. The ratios show little sensitivity to pre-heat temperatures below 270 °C, and have no strong dependence on test dose size.

2.2.3. Luminescence depth profiles

Profiles of luminescence with depth into a clast are used to ascertain whether a clast surface was bleached before burial. A good indication of bleaching is the presence of a plateau in Ln/Tn for the first few slices, showing that these slices were fully bleached before burial. In previous work, the profiles have been fitted using a theoretical model to aid identification and extent of the bleaching plateau, and with further short cores drilled to assess the burial dose to the outer slices (e.g. Souza et al., 2019; Rades et al., 2018). In this study, we measure a greatly increased number of clasts (in order to increase the probability of finding well-bleached clasts), but a limited number of cores for each clast (due to sampling constraints). We therefore seek to reduce the measurement time required to date any one clast, and so we exploit the luminescence depth profiles for both the analysis of bleaching and burial-dose estimation. We design a simplified fitting procedure for this purpose, assuming that there is only one burial event of interest. The dose-response curve is subsequently measured for a single slice of each core. Sohbati et al. (2012) and Freiesleben et al. (2015) have provided a framework for the fitting of bleaching and burial-dose models to the Ln/Tn depth profile, incorporating repeated bleaching and burial events. For a single bleaching and single burial, the normalised model takes the form:

$$L(x) = \left(e^{-t_e\overline{\sigma\varphi}e^{-\mu x}} - 1\right)e^{-F(x)t_b} + 1 \quad (1)$$

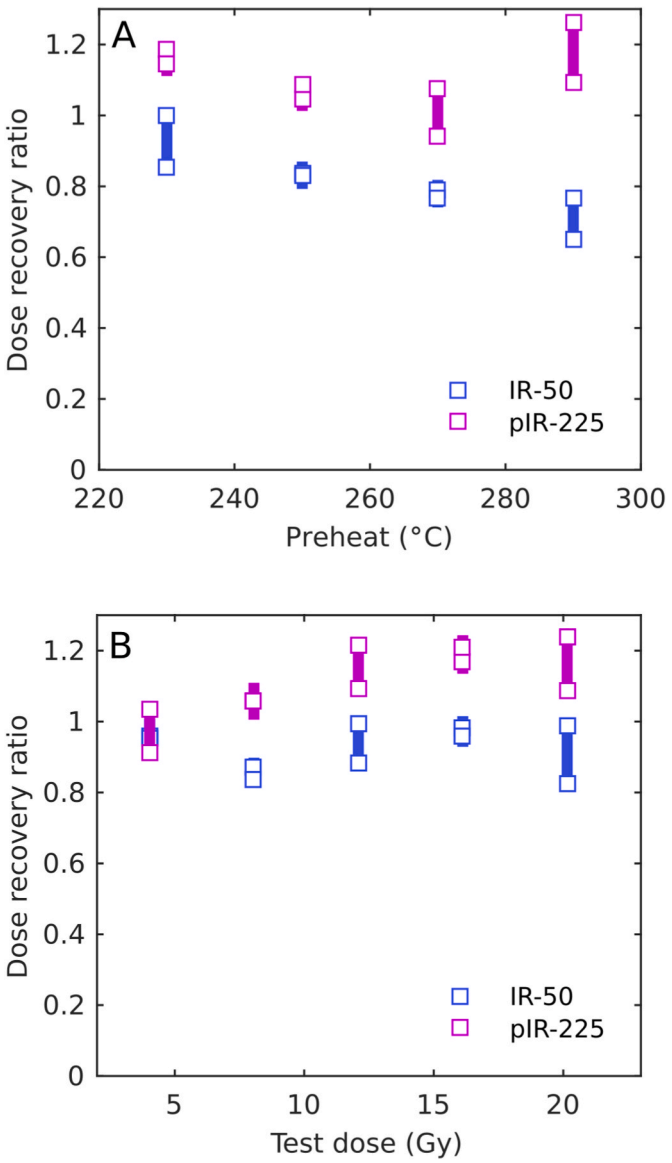

Fig. 3. Sensitivity of the ratio of recovered dose (60 Gy) to given dose, to preheat temperature and size of test dose. (a) Dose recovery ratio against preheat temperature for sample T8-6, using test dose of 12 Gy. (b) Dose recovery ratio against test-dose size for sample T4-1, using a preheat of 250 °C.

where t_e is the exposure time (before burial), σ is the photo-ionisation cross section, φ is the bleaching photon flux, μ is the light attenuation with depth, t_b the length of burial, F(x) is the trap filling rate and assumed proportional to the dose. Since this is a single bleaching event, t_e, σ and φ are all constants, and cannot be separated. Thus the term $t_e\overline{\sigma\varphi}$ can be treated as a single constant, F_{bleach}, describing the total amount of bleaching before burial. Similarly, t_b and F(x) cannot be separated without prior knowledge, and for our purpose the dose rate can be considered independent of depth (see section 2.5). Thus we can assign a single constant, F_{dose}, to describe dose accumulation. When applied to unnormalised data, the model requires a constant scale factor, L_{sat}, which is the luminescence signal at saturation. With these simplifications, the equation can be written:

$$L(x) = L_{sat}\left(\left(e^{-F_{bleach}e^{-\mu x}} - 1\right)e^{-F_{dose}} + 1\right) \quad (2)$$

which has four free parameters (L_{sat}, μ, F_{bleach} and F_{dose}). The model is fitted to both the IR_{50} and $pIRIR_{225}$ profiles using the Bayesian computational programming language *Stan* (Carpenter et al., 2017). The

model fit is created for each core using multiple Markov chains, with convergence monitored using the $\widehat{R}$ statistic (Gelman and Rubin, 1992). Formulating the model this way allows prior information on the parameters to be included, if desired, and provides a posterior distribution of parameter values. Here, we use non-informative priors for F_{bleach}, F_{dose} and L_0 (i.e. unconstrained fitting), and also for μ in the case of IR_{50} data. For the $pIRIR_{225}$, we choose to constrain μ using the posterior μ from the IR_{50} fit for the same profile – thus forcing the shape of the $pIRIR_{225}$ profile to be similar to that of the IR_{50}. The parameter μ — the rate of change in signal depletion with depth — is a function of the light attenuation characteristics of the rock, but may also be affected by the wavelength dependence of bleaching of different luminescence signals (Ou et al., 2018; Meyer et al., 2018). As we are considering two very similar signals from the same mineral, we presume here that rock characteristics are the dominant control on μ. For dose estimation, we define L_B, derived from the fitted parameters of the model:

$$L_B = L_{sat}\left(1 - e^{-F_{dose}}\right) \quad (3)$$

where L_B represents the portion of L derived only from the burial dose (i.e. after removal of any non-bleached component left at the time of burial). Thus, by assuming μ is dependent only on rock characteristics, we can, in principle, use the value of L_B to derive burial dose estimates even from cores that have not been completely bleached at the surface.

2.2.4. Fading

Any anomalous fading of the feldspar signal can be assessed using the luminescence profiles. For most of the cores measured, the innermost slices are unaffected by light penetration, and so the luminescence signal will be in field saturation – i.e. in a dynamic equilibrium between trap filling (from dose rate) and trap emptying (from fading). When a radiation dose is given and the resulting luminescence measured on a laboratory timescale (minutes), fading is not significant, and so the luminescence signal is greater than that corresponding to the same natural dose. If this laboratory dose is large (a saturation dose), then the ratio of the natural luminescence response to a saturation dose, to the laboratory luminescence response – the saturation ratio – gives a direct measure of the upper limit to the effect of fading on the natural luminescence; this ratio can then be used to correct the burial-dose luminescence signal for anomalous fading. For example, Fig. 4a shows the IR_{50} depth profile for sample T5-7-A1, together with the Bayesian fit of equation (2), and the inferred profile at the time of deposition. The three deepest slices were given a saturation dose of ~2000 Gy and re-measured; the average saturation ratio, defined by $(L_n/T_n)/(L_{sat}/T_x)$ (i.e. the field saturation as a proportion of the laboratory saturation), was is 0.86 ± 0.03. This ratio is used to correct the burial dose luminescence signal, L_B, before projecting onto the dose-response curve (Fig. 4b).

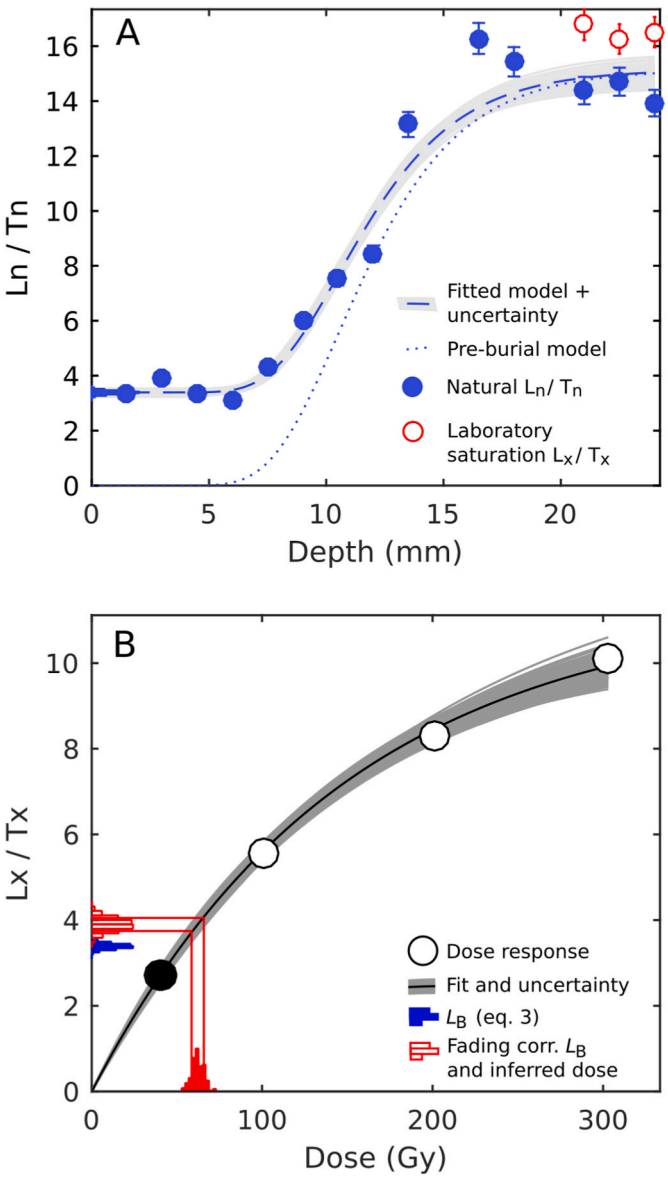

Fig. 4. Illustration of the burial dose estimation procedure using the IR_{50} signal from core T5-7-A1. (a) Burial dose profile, fitted with eq. (2); also shown is the pre-burial component of the fitted model, giving a visual confirmation of the bleaching depth (>5 mm in this case). (b) Dose estimation using the L_B derived from the fitted burial profile (eq. (3)). L_B is corrected for fading using the laboratory saturation ratio, and projected onto the dose-response curve.

2.3. Dose rate

The dose rate to feldspar grains in rock slices is provided by the decay of naturally occurring radionuclides of K, U and Th, contained within minerals of the rock itself or the surrounding sediment. The range of beta radiation in rock is ~1.5 mm (Riedesel and Autzen, 2020), so except for the surface slice the beta contribution comes entirely from within the clast. The maximum range of gamma photons in rock is of the order of 20 cm; we can expect that a maximum of 50% of the gamma dose rate to layers at or close to the rock surface is derived from the clast, with the rest from the surrounding matrix (clasts and sediment). The primary challenge is to estimate the bulk, infinite matrix, beta and gamma dose rates to the clast. Typically, this is calculated using the activity concentrations measured with HpGe gamma spectrometry (e.g. Rades et al., 2018; Souza et al., 2019). However, such measurements usually require relatively large samples (20–250 g) of both the clast and the matrix. In our case, the mass of clast material available is mostly in the range of 5–10 g. This quantity is sufficient for thick source beta counting, so we seek to exploit the recent advances in beta counting methodology and develop a procedure suitable for rock surface dating.

Cunningham et al. (2018) described a beta counting procedure that provides precise and accurate dose rate estimates using small sample sizes. Following Ankjaergaard and Murray (2007), samples are pulverised to produce a homogenous powder, embedded in wax for radon retention, and stored for several weeks to allow radon daughters to equilibrate. Calibration samples are prepared from recognised standards for K, U and Th (Murray et al., 2018), with correction applied to account for the differences in electron stopping power between wax and sediment. The prepared samples consist of 3–5 small sub-samples, of various proportions of wax/sediment, requiring a total sediment mass of <10 g. These sub-samples are measured on one of 4 Risø low-level beta counters for ~24 h, with count rates corrected for detector sensitivity and background.

The measured beta count rate for a sample is dependent on the source radionuclide, because the count rates per unit dose rate are different for K, U, and Th sources. Cunningham et al.'s solution is to use prior information on the K, U, Th (i.e. data from another source) to create a unique calibration factor for each sample. Importantly, the method does not require knowledge of the absolute concentrations of K, U and Th, only their relative proportions. These proportions are estimated here using a simplified version of the gamma spectrometry procedures described in Murray et al. (1987, 2018). Here, we measure the gamma spectrum for each clast using whatever material is available, placed in an irregular geometry. The material may include a mix of measured slices, wax-embedded powder prepared as sub-sample 'buttons' for beta counting, or unmeasured cores wrapped in light-tight plastic. The photo-peak count rates are converted to (nominal) activity concentration by reference to a planar-geometry calibration. The relative activity concentrations of K, U and Th can then be derived, assuming secular equilibrium in the U and Th chains. The assumption here is that the relative counting error caused by using a poorly-defined geometry (with respect to the standards) is the same for each of the main photo-peaks used. This assumption is likely to hold for all photons which are not substantially absorbed by the samples, so that the effects of poorly-defined counting geometries are primarily geometrical and so independent of energy; for a 1 cm thick sample of solid quartz, the attenuation over the energy range of interest, i.e. from 200 keV to 1500 keV, is between only ~5 and ~2%. For granite cobbles, secular equilibrium during burial is almost certain; the cobble is essentially chemically unaltered for a period far longer than the longest progeny half-life in the U or Th chains, and radon loss can safely be assumed to be minimal because radon mobility is a function of porosity (Tanner et al., 1980). Likewise, during measurement radon is likely retained within the rock cores, or within the wax-embedded beta buttons.

2.3.1. Dose rate calculations

Beta and gamma dose rate estimates use the conversion factors of Guerin et al. (2011). The beta dose rate is assumed constant for all slices in the clast. We add feldspar beta self-dose of 1.4 ± 0.2 Gy ka^{-1}, based on a K-feldspar grain size of 400 μm and 12% potassium, with the beta attenuation factors of Guérin et al. (2012). The grain size and K percentage were estimated from micro-XRF imaging of selected rock slices, following the procedure of Rades et al. (2018). For the gamma dose rate, we presume an equal weight in the contributions from the clast and the surrounding sediment. For the Baksan debris fans, the mass of the surrounding sediment is overwhelmingly dominated by other cobbles. The external portion of the gamma dose rate is estimated by the average of all the measured clasts for the sampling location (between 3 and 5 cobbles). The cobbles are locally derived and have a consistent lithology. The internal and external gamma dose rates are similar, so there is no need to model the gamma radiation field (c.f. Sohbati et al., 2015). Similarly, the water content is negligible and no correction to the dose rate is required. The cosmic and alpha contributions to the dose rate are negligible and are also omitted.

2.4. Rangefinder ages for site 4

A small river-cut debris cone at Site 4 is used to test an alternative measurement strategy that avoids profile measurements altogether, but relies on statistical analysis of D_e derived from individual slices of multiple clasts. Due to problems with the bench-top drill press, only short cores of ~1 cm could be obtained from clasts of this site. The cores are too short to obtain a full bleaching profile, so the profile fitting routine of Section 2 could not be applied. Instead, short cores were drilled in each buried face of the clast, and the D_e was measured for the second slice of each core only, evaluated with the IR_{50} signal. Although in principle the first slice is the most likely to be well bleached, it is often misshapen (i.e. of poorly defined thickness) or disintegrates during slicing; avoiding slice 1 also simplifies the beta dose rate calculation. Dose rates for each clast are estimated through beta counting (as in Section 2.2), with prior information on relative K, U, Th concentrations estimated from gamma-spectrometry of several clasts at the site. Without a full profile, fading rates must be estimated from laboratory fading measurements. The average g-value measured from 17 slices was 3.1 ± 0.9; we use a common fading correction to all slices (incorporating the uncertainty), following the correction procedures of Huntley and Lamothe (2001) and Auclair et al. (2003). The apparent age of the slices can then be estimated, and grouped by the sampling unit (2–3 clasts each; Fig. 9b).

In a full burial profile, the presence of an Ln/Tn plateau can help to identify clasts that were bleached before burial. Single slices have no such control, and their apparent ages are treated here as statistically independent. In this way, the distribution of apparent ages for the slices in a given sampling unit is analogous to a poorly bleached distribution of D_e measured on sand grains or small aliquots. The distribution can be considered a mixture of two normal populations: (1) representing the well-bleached slices, with a narrow distribution centred on the mean, ν, with the standard deviation τ_1; (2) representing the slices that have an additional residual dose, ε, centred on the mean, $(\nu + \varepsilon)$, with standard deviation τ_2. The mixture model for the distribution of apparent ages of the slices, θ, can be described by:

$$p(\theta) = qN(\nu, \tau_1) + (1 - q)N(\nu + \varepsilon, \tau_2) \quad (4)$$

where $N(.)$ represents the normal distribution, q is the weights of the mixture, and ν is the burial age for each sedimentary unit (ka). All slices from within a unit are treated as a single distribution. The burial dose for each slice is converted into apparent age by dividing by the dose rate for the clast, hence ν, ε, τ also have units of ka. The model is conceptually similar to the four-component minimum-age model of Galbraith et al. (1999) and in practice similar to that of Tamura et al. (2018). In addition, we put age-order constraints on ν, forcing the age estimates to conform to stratigraphic order, and prior constraint on τ_1 to limit the expected scatter on the well-bleached population.

3. Results

3.1. Site 1: Colluvium

Good burial profiles were obtained from the IR_{50} signal from almost all clasts sampled at site 1; for many clasts, a bleaching plateau is also seen in the pIR_{225} profile (Fig. 5); the fitted models predict that many were well-bleached before burial, in some cases to depth of more than 7 mm (e.g. Fig. 5: T4-3-A1.). The saturation ratios are consistent between clasts, and indicate a low degree of anomalous fading. The average ratios are ~0.93 for $pIRIR_{225}$ signal, and ~0.87 for the IR_{50}. For some clasts the saturation ratio was not measured, and these average ratios were used instead (Table 1). Clast dose rates are relatively high, ranging from 4.5 to 9.5 Gy ka^{-1}. The fading-corrected burial-age estimates for each core are plotted as probability densities (Fig. 6). IR_{50} ages for clasts at location T6 and T7 are very consistent, despite the range in dose rates across clasts, indicating that the burial-doses are reliable. The $pIRIR_{225}$ ages are more erratic due to the shorter bleaching profile, but generally support the IR_{50} ages. Locations T5 and T6 lie roughly halfway between the surface of the deposit and the valley floor; the burial ages cluster around 6–8 ka. At the surface location T8, three clasts provide consistent burial ages of <1 ka. The stratigraphically lowest location, T4, provides inconsistent burial ages across the samples measured. Two clasts provide burial ages consistent with, or slightly older than, locations T5 and T6, and two clasts provide ages that are not credible given the wealth of data from overlying sediments. We speculate that the sediment at T4 was actually disturbed, as it lies just above the landslip unit, and that this disturbance was not identified in the field. Burial ages for location T7 in landslip unit are ~5 ka for two clasts, with a third clast reflecting an older bleaching event. This suggests that the landslip unit originally lay

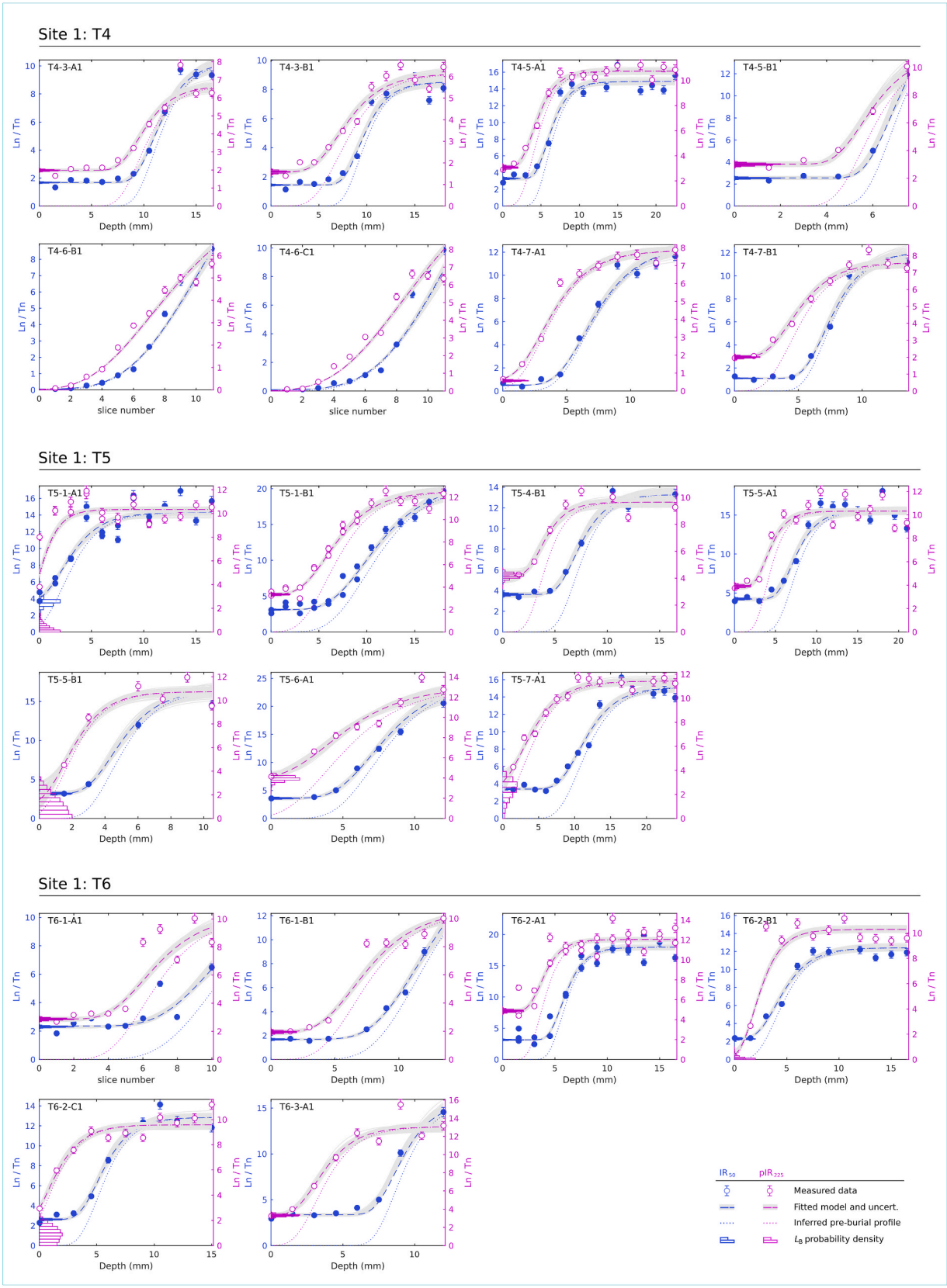

Fig. 5. Luminescence depth profiles for cores sampled from clasts from Site 1 (locations T4, T5, T6, T7, T8), Site 2 (T1), and Site 3 (T3). Each plot shows data for a single core. In most cases, more than one face of a clast was cored. Plots are labelled using the core ID, in the format [location]-[clast]-[Face + core]; e.g. T6-3-A1 is the first core drilled in face A of clast 3, taken form location T6. Data and fitted models are shown for IR_{50} and $pIRIR_{225}$ signals. The fitted model is used to derive L_B, the inferred signal resulting from the burial dose, indicated by the histograms. Where the bleaching profile is short, the inferred L_B may be very imprecise – this is most apparent for the less-bleachable $pIRIR_{225}$ signal.

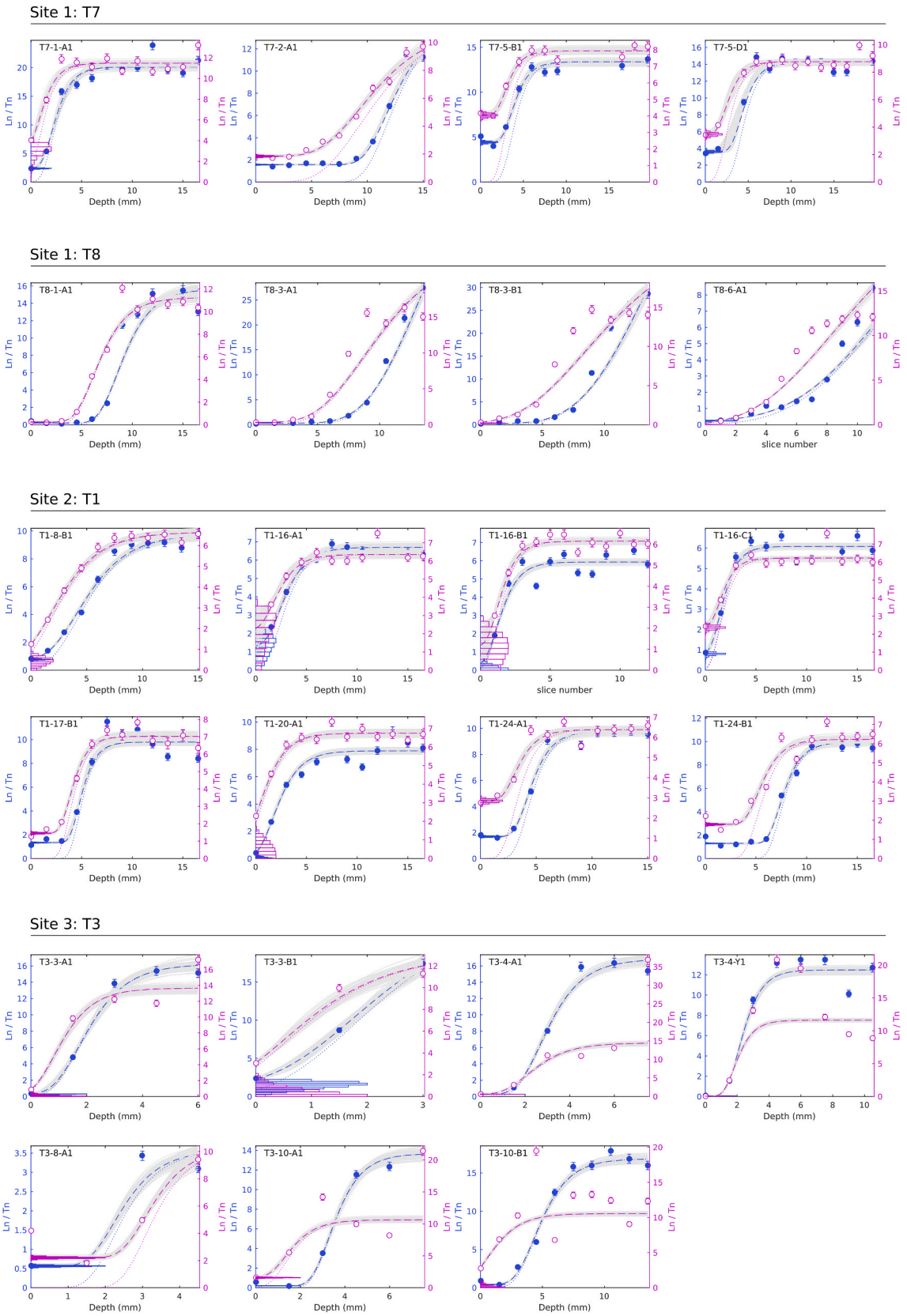

Fig. 5. (*continued*).

much higher in the section, stratigraphically above T5 and T6.

In summary, it seems likely that the bulk of the sediment in the colluvial cone was deposited in the early Holocene, between 5 and 10 ka. However, the young ages for cobbles close to the surface (T8), and the observed cobble lobes on the surface, indicate that deposition continues to the present. Note also that there are no burial ages for the true base of

Table 1
Equivalent dose, dose rates, and ages estimated for each measured core from Sites 1–3. For most clasts, ages have be calculated for two or more cores. Cores identifiers use the format [location]-[clast]-[Face + core]. Saturation ratios are shown for cores where measured; site-averaged values are used for the remainder.

Clast	*Equivalent dose*		*Saturation ratio*		*Clast Dry dose rate (Gy ka-1)*				
	IR De (Gy)	*pIR De (Gy)*	*IR Sat*	*pIR Sat*	*beta*	*gamma*	*Dr (Gy ka-1)*	*IR Age (ka)*	*pIR Age (ka)*
T1-8-B1	29.5 ± 2.1	12.4 ± 5.9	0.43 ± 0.01	0.57 ± 0.02	2.48 ± 0.06	0.84 ± 0.03	4.46 ± 0.28	6.6 ± 0.61	2.8 ± 1.35
T1-16-A1	133.2 ± 92.9	103.9 ± 62.9	0.3 ± 0.01	0.56 ± 0.02	1.38 ± 0.05	0.51 ± 0.02	3.29 ± 0.26	40.97 ± 29.01	31.98 ± 19.44
T1-16-B1	14.6 ± 12.4	41.9 ± 26.8	0.3 ± 0.01	0.56 ± 0.02	1.38 ± 0.05	0.51 ± 0.02	3.29 ± 0.26	4.45 ± 3.84	12.72 ± 8.24
T1-16-C1	53.9 ± 5.7	111.6 ± 10.8	0.3 ± 0.01	0.56 ± 0.02	1.38 ± 0.05	0.51 ± 0.02	3.29 ± 0.26	16.48 ± 2.21	33.97 ± 4.01
T1-17-B1	58.3 ± 5.6	52.8 ± 3.6	0.35 ± 0.03	0.51 ± 0.02	1.65 ± 0.06	0.61 ± 0.02	3.59 ± 0.26	16.4 ± 2.08	14.73 ± 1.49
T1-20-A1	2.3 ± 1.8	15.7 ± 11.4	0.46 ± 0.04	0.71 ± 0.04	2.60 ± 0.11	1.01 ± 0.04	4.66 ± 0.3	0.50 ± 0.40	3.37 ± 2.44
T1-24-A1	51.6 ± 3.2	112.9 ± 15.1	0.41 ± 0.02	0.53 ± 0.03	1.80 ± 0.02	0.66 ± 0.02	3.75 ± 0.26	13.91 ± 1.3	30.2 ± 4.57
T1-24-B1	42.7 ± 2.5	62.2 ± 5.7	0.41 ± 0.02	0.53 ± 0.03	1.80 ± 0.02	0.66 ± 0.02	3.75 ± 0.26	11.3 ± 1.04	16.59 ± 1.86
T4-3-A1	42.2 ± 2.0	60.9 ± 3.4	0.9 ± 0.03	0.93 ± 0.03	2.76 ± 0.08	1.47 ± 0.04	6.14 ± 1.48	7.36 ± 2.15	10.67 ± 3.38
T4-3-B1	36.1 ± 1.9	42.9 ± 2.5	0.9 ± 0.03	0.93 ± 0.03	2.32 ± 0.07	1.24 ± 0.04	5.62 ± 1.45	7.55 ± 3.61	8.66 ± 4.24
T4-5-A1	68.2 ± 3.3	66.6 ± 5.8	0.78 ± 0.02	0.88 ± 0.04	2.27 ± 0.08	1.25 ± 0.04	5.58 ± 1.38	13.42 ± 3.88	12.59 ± 3.59
T4-5-B1	49.6 ± 2.4	61.4 ± 4.5	0.78 ± 0.02	0.88 ± 0.04	2.27 ± 0.08	1.25 ± 0.04	5.58 ± 1.38	9.70 ± 2.98	11.94 ± 3.93
T4-6-B1	1.3 ± 0.1				3.91 ± 0.06	6.03 ± 0.10	9.47 ± 1.4	0.14 ± 0.03	
T4-6-C1	2.4 ± 0.2	0.1 ± 0.1			3.91 ± 0.06	6.03 ± 0.10	9.47 ± 1.4	0.25 ± 0.04	0.02 ± 0.01
T4-7-A1	13.5 ± 1.8	14.9 ± 1.2	0.94 ± 0.03	0.93 ± 0.03	3.08 ± 0.06	1.49 ± 0.05	6.44 ± 1.38	2.24 ± 0.61	2.50 ± 0.78
T4-7-B1	27.6 ± 1.3	60.1 ± 3.5	0.94 ± 0.03	0.93 ± 0.03	3.08 ± 0.06	1.49 ± 0.05	6.44 ± 1.38	4.48 ± 1.22	9.63 ± 2.30
T5-1-A1	66.8 ± 10.0	5.6 ± 5.1			4.65 ± 0.08	1.71 ± 0.03	7.77 ± 0.44	8.62 ± 1.37	0.73 ± 0.66
T5-1-B1	57.6 ± 3.6	66.5 ± 3.4			4.65 ± 0.08	1.71 ± 0.03	7.77 ± 0.44	7.43 ± 0.63	8.56 ± 0.63
T5-4-B1	71.8 ± 4.7	91 ± 6.7			4.46 ± 0.05	3.07 ± 0.03	8.27 ± 0.45	8.71 ± 0.72	11.07 ± 1.02
T5-5-A1	78.0 ± 3.6	81.4 ± 4.9	0.92 ± 0.03	0.91 ± 0.02	5.30 ± 0.16	2.87 ± 0.09	8.94 ± 0.49	8.73 ± 0.68	9.12 ± 0.72
T5-5-B1	55.2 ± 3.1	21.0 ± 15.3	0.92 ± 0.03	0.91 ± 0.02	5.30 ± 0.16	2.87 ± 0.09	8.94 ± 0.49	6.16 ± 0.46	2.35 ± 1.71
T5-6-A1	73.1 ± 5.1	92.9 ± 9.3			4.69 ± 0.08	2.12 ± 0.04	8.01 ± 0.45	9.16 ± 0.8	11.68 ± 1.36
T5-7-A1	63.5 ± 3.3	44.4 ± 17.2	0.86 ± 0.03	0.95 ± 0.03	4.96 ± 0.15	2.56 ± 0.08	8.48 ± 0.47	7.49 ± 0.59	5.25 ± 2.04
T6-1-A1	48.1 ± 2.9	62.4 ± 3.4			4.10 ± 0.06	2.07 ± 0.03	7.23 ± 0.39	6.64 ± 0.54	8.66 ± 0.68
T6-1-B1	46.8 ± 3.1	53.7 ± 3.1			4.10 ± 0.06	2.07 ± 0.03	7.23 ± 0.39	6.49 ± 0.55	7.42 ± 0.58
T6-2-A1	47.6 ± 2.9	90.6 ± 5.0			3.22 ± 0.05	2.01 ± 0.04	6.39 ± 0.37	7.46 ± 0.6	14.18 ± 1.14
T6-2-B1	47.1 ± 3.2	2.3 ± 2.3			3.22 ± 0.05	2.01 ± 0.04	6.39 ± 0.37	7.39 ± 0.64	0.36 ± 0.36
T6-2-C1	55.3 ± 3.4	17.3 ± 11			3.22 ± 0.05	2.01 ± 0.04	6.39 ± 0.37	8.70 ± 0.74	2.73 ± 1.72
T6-3-A1	61.0 ± 3.5	54.4 ± 3.4	0.87 ± 0.03	1.02 ± 0.04	4.24 ± 0.13	2.35 ± 0.07	7.50 ± 0.90	8.27 ± 1.1	7.40 ± 0.99
T7-1-A1	42.5 ± 3.1	59.3 ± 14.3			5.67 ± 0.07	2.46 ± 0.03	8.87 ± 0.62	4.81 ± 0.5	6.70 ± 1.69
T7-2-A1	28.0 ± 1.6	34.0 ± 2.0	0.82 ± 0.03	0.91 ± 0.03	1.76 ± 0.04	0.93 ± 0.02	4.51 ± 0.56	6.3 ± 0.94	7.65 ± 1.15
T7-5-B1	103.6 ± 7.9	135.2 ± 15.7	0.82 ± 0.03	0.82 ± 0.03	2.72 ± 0.05	2.78 ± 0.05	6.32 ± 0.58	16.48 ± 1.92	21.5 ± 3.31
T7-5-D1	70.5 ± 5.4	86.3 ± 7.0	0.82 ± 0.03	0.82 ± 0.03	2.72 ± 0.05	2.78 ± 0.05	6.32 ± 0.58	11.21 ± 1.38	13.69 ± 1.71
T8-1-A1	2.8 ± 0.2	3.7 ± 0.2	0.91 ± 0.03	0.93 ± 0.03			7.09 ± 0.39	0.40 ± 0.03	0.52 ± 0.04
T8-3-A1	4.9 ± 0.3	5.1 ± 0.2			3.19 ± 0.06	2.06 ± 0.05	6.38 ± 0.37	0.78 ± 0.06	0.81 ± 0.06
T8-3-B1	4.2 ± 0.3	3.1 ± 0.4			3.19 ± 0.06	2.06 ± 0.05	6.38 ± 0.37	0.66 ± 0.06	0.49 ± 0.06
T8-6-A1	3.8 ± 0.3	0.2 ± 0.1					7.09 ± 0.39	0.53 ± 0.06	0.02 ± 0.02

Table 2
Modelled burial ages for the sampled units of debris cone, Site 4. The high apparent age of the modern channel sediment implies a high residual dose (i.e. age offset) in the debris units; as such, the ages given should be treated with caution.

Unit	*Description*	*Age (ka)*
1	Modern Channel	0.65 ± 0.06
2	Debris flow	0.69 ± 0.06
3	Debris Flow	0.77 ± 0.05
4	Debris Flow	0.85 ± 0.06
5	Fluvial	1.55 ± 0.28

the debris fan, leaving the date of onset uncertain.

3.1.1. Site 2: Tyubella swell debris cone

We sampled cobbles from a debris-cone section of the Tyubele swell, adjacent to the road. Very few clasts at this site showed significant evidence of bleaching prior to burial. Of the five that were retained for further analysis (Table 1; Fig. 7), only two clasts show a convincing burial-dose plateau at the surface (T1-17 and T1-24). Laboratory saturation ratios were measured for all five clasts, and lie in the range 0.3–0.5 for the IR_{50} signal, and 0.5–0.7 for the $pIRIR_{225}$. The large fading correction applied to these clasts inevitably leads to a relatively large uncertainty in the age estimate. Of the two most convincing clasts, T1-17 gives comparable ages for IR_{50} and $pIRIR_{225}$ of ~15 ka, and clast T1-24 has cores from two faces giving ages in the range of 10–20 ka. These clasts are indicated by filled histograms in Fig. 7. Where the pre-burial bleaching of clasts is incomplete, the inferred ages are much less precise: these are indicate in Fig. 7 using open histograms.

3.1.2. Site 3: Active debris flow of the Sagayevsky stream

Several clasts were collected from the most recent debris flow in the valley and were intended to serve as modern analogues of buried material elsewhere. Short profiles were obtained from 4 clasts, from which we obtained the modern residual dose. A bleaching profile is seen in all of the cores measured, but none have a well-developed plateau (see Fig. 5: Site 3 plots). This suggests that bleaching may not be complete in the surface slices. The residual doses lie in the range 0–6 Gy for IR_{50} and $pIRIR_{225}$ (before fading correction), which is equivalent to ~1 ka of the typical burial dose. One (short) core shows some evidence of a burial-dose plateau, indicating that the clast had a prolonged burial after initial erosion and transport, and was then re-entrained in the modern debris flow. Two clasts show much larger $pIRIR_{225}$ burial doses.

3.1.3. Site 4 – Small debris cone

Clasts were sampled from three debris-flow beds, the channel, and the underlying fluvial cobbles (Fig. 9a). Analysis of this site follows the alternative strategy described in Section 2.4, for when bleaching profiles are not obtainable. Approximate burial ages are shown in Fig. 9 for each

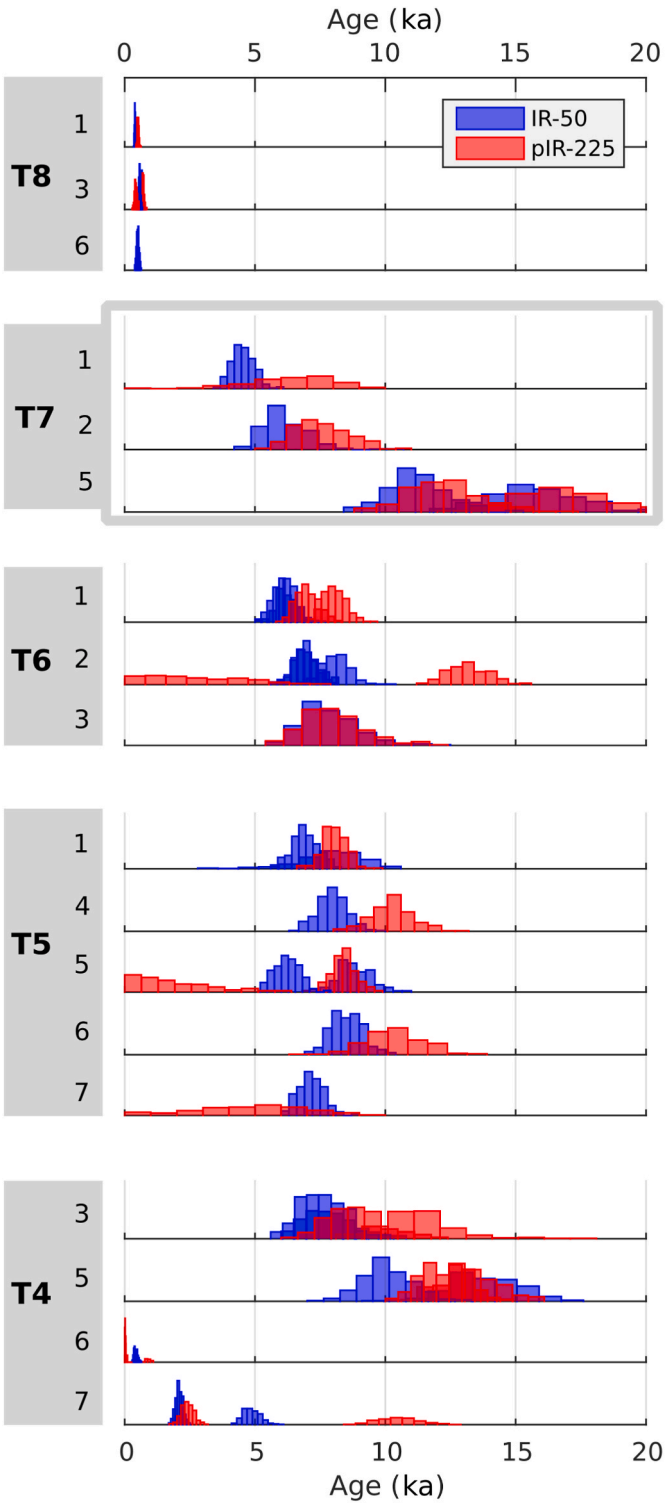

Fig. 6. Burial ages for the hillslope debris fan Site 1, showing fading-corrected IR_{50} and $pIRIR_{225}$ ages, plotted as probability densities. Each row shows results from a single clast; some clasts have ages determined for more than one core. Sampling locations are plotted in stratigraphic order (lowermost T4, uppermost T8). The original position of the land-slipped T7 is uncertain and is plotted here above T6 *post hoc* on the basis of the burial ages. Within each location, samples are plotted by (arbitrary) sample number.

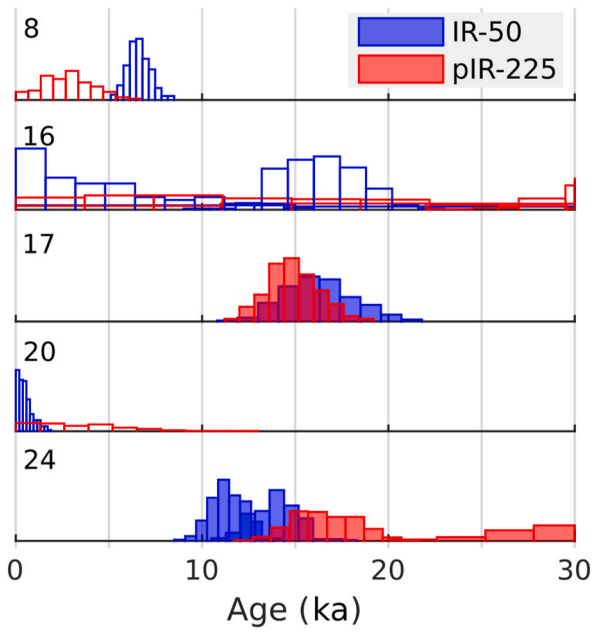

Fig. 7. Burial ages for 4 clast of Site 2, the Tyubele Swell, plotted as probability densities. Plots are ordered by clast number, and no stratigraphic ordering is implied. Filled histograms indicate cores where the modelled pre-burial profile shows complete bleaching at the surface (see Fig. 5: T1-17-B1; T1-24-A1; T1-24-B1). Open histograms are used for the remaining cores from the site; these cores do not show full pre-burial bleaching.

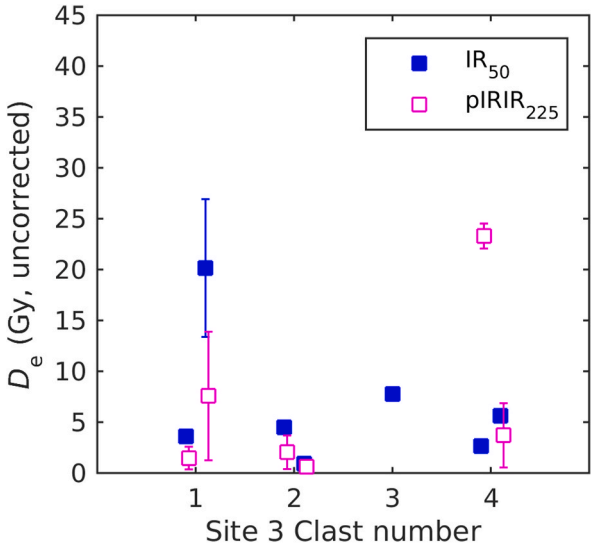

Fig. 8. Burial doses obtained from four clasts of the modern debris-flow sediment at Site 3, shown for both the IR_{50} and pIR_{225} signals.

measured slice (the second slice from each core), together with the modelled burial ages (as outlined boxes) for each unit. The modelled ages for the debris-flow units range from c. 850 years–690 years, with the underlying fluvial unit estimate at ~1500 years. However, the modelled age for the modern channel sediment is also ~650 years, presumably as a result of an unbleached residual in all the measured clasts (i.e. none were completely reset). If so, a residual dose equivalent to ~650 years can also be expected in the debris flow units, and so it seems very likely that the debris cone was deposited recently, over the last few hundred years (Fig. 9b). This is very encouraging for future work, as such small offsets imply it is very likely that useful chronological information can be obtained from other, older debris cones of

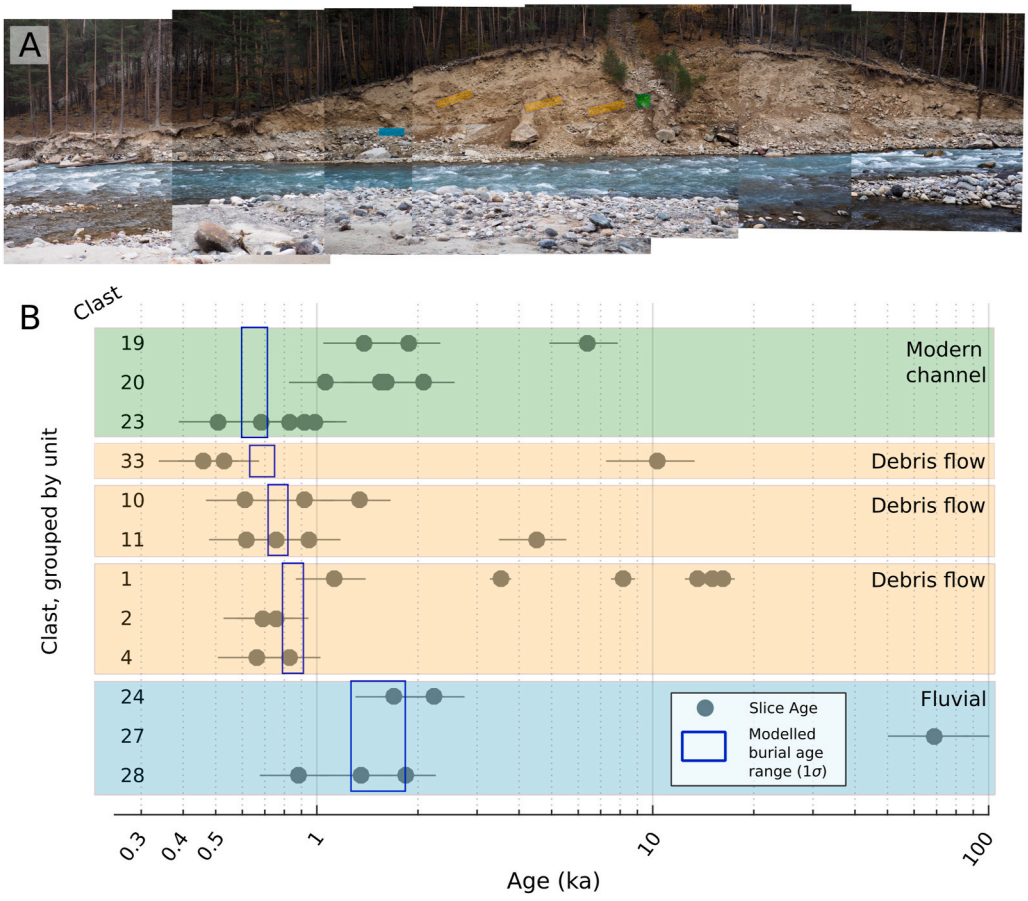

Fig. 9. Burial ages estimated for Site 4 (debris cone) using a statistical model of the apparent ages for the clasts. (a) Composite photo of the debris cone, with the sampled units indicated by coloured shading. (b) Apparent ages plotted by clast number. Each point represents a single measured slice from different core. Each row shows the slices for a single clast. Clasts are grouped by the sedimentary units, shaded using the same colour scheme as (a). Units are plotted in stratigraphic order; within units, samples are plotted by (arbitrary) clast number. The modelled burial age range for each unit is also shown (modelled ages are constrained by stratigraphic order).

this type. Nevertheless, the absolute ages presented for Site 4 can only be considered approximate: the number of samples is small for a statistical model; and as with other types of poor-bleaching model, the result is sensitive to the assumed dispersion in the well-bleached component.

4. Discussion

Of the clasts sampled from the colluvial Site 1, the bulk provide age estimates in the range of 6–8 ka. The sampling locations at site 1 were chosen by their accessibility, so the possibility of sampling bias must be recognised. Nevertheless, these ages are consistent with the warmest and wettest period of the Holocene in the wider Caucasus region (6–8 ka, Connor and Kvavadze, 2009). Lake sediments from the western Caucasus mountains show an increase in biological productivity between 8.0 and 6.7 ka cal BP, with pollen assemblages indicating an expansion of low and mid-altitude forests into high mountain areas (Grachev et al., 2020). Climate reconstruction in the Lesser Caucasus range show a similar pattern, with the onset of peak conditions at 8.2 ka (Joannin et al., 2013). Data is more sparse in the central Caucasus: pollen analysis of peatlands have indicate two warm stages at 7500-5500 BP and 5000-3100 BP (uncalibrated ^{14}C, Knyazev et al. (1992)); and a phases of glacier retreat from 8600 to 6400 BP (uncalibrated ^{14}C, Serebryaniy et al., 1984). Warmer and wetter climates are associated with increased weathering, so it is likely that the production of colluvium was greater in the early-to-mid Holocene.

The dating of the Tyubele swell (Site 2) was much less successful, with only two clasts giving reliable ages in the broad range of 10–20 ka. The clasts were sampled from a debris cone underlying unstructured sediment. The ages are broadly consistent in time with deglaciation, but offer little further information. Ages for the active debris cone on site 4 are also consistent with expectations, although they offer little precise information on debris flow activity. What is most interesting is the potential of rock-surface methods to date the deglaciation of the region. There are very few preserved moraines in the region, but a systematic programme of dating colluviam and debris cones may provide a chronology of glacial retreat, assuming these features are taken to post-date glacial activity. However, improvements will be needed in sampling and measurement efficiency.

The usefulness of the dating method depends on whether the clasts have a good probability of bleaching before burial, and there is reason to be optimistic. Clasts from the large colluvial cone (Site 1) show a high degree of bleaching. Almost every clast cored shows a bleaching profile in the IR_{50} signal, often on two or more faces. The IR_{50} signal shows a bleaching plateau that indicate full bleaching to a depth of 3–6 mm in the majority of cores (Fig. 5). In many cases the less bleachable but more stable $pIRIR_{225}$ signal is also shows a burial-dose plateau, with full signal resetting to a depth of 1–3 mm. For the debris-flow sediment, the degree of bleaching is more variable. Short profiles were measured from a modern debris flow (Site 3), all of which show some degree of bleaching of the IR_{50} signal at the surface. However, none of the cores show a bleaching plateau comparable to that of the colluvial clasts. The residual dose estimated from the IR_{50} for 4 clasts lies in the range of 1–8 Gy, slightly more than the doses measured in the most recent buried clasts from Site 1 (T8: 3–5 Gy). The debris flow clasts in the Tyubele swell section (Site 2) display the least bleaching of any of the sites examined. Very few clasts showed any kind of bleaching at the surface, and only two clasts can be considered reliable, albeit imprecise (clasts with saturated profiles are not shown in the figures).

The differences in bleaching between the sites could reflect local variables like aspect and lithology, or they might reflect the different transport pathways for the clasts involved. The source area for the Site 1 colluvium is south-facing, while the valley catchments of the debris

flows are broadly north-facing. All clasts have broadly the same lithology, but differences in (e.g.) grain size or shape could conceivably effect light penetration. The observation that bleaching at site 1 occurs on more than one face of each clast suggests that there is a significant period of surface transport after erosion from the bedrock, but without sub-surface burial. In contrast, the debris-flow sediments (Sites 2,3,4) have a more extensive source areas in the tributary valleys. The source material may well include colluvium, but is also likely to include glacial debris from Little Ice Age moraines, and from the extant glaciers. While it is likely that many glacially eroded clasts receive sunlight exposure, eroded clasts might also be buried for long periods before entrainment in a debris flow. Prolonged burial would lead to a build-up of the luminescence signal, with no further bleaching likely during debris-flow transport.

Our initial uncertainty about the likelihood of finding good profiles led to several innovations in measurement strategy, with the aim of increasing the number of clasts measured. The rationale was that a greater number of clasts would give statistical rigour, even if there was a cost in measurement precision. Profiles were measured using a post-IR protocol, which provides two measurable signals – the IR_{50} and (in this case) the $pIRIR_{225}$. Of these, the IR_{50} is easier to bleach and so more likely to be fully reset, but $pIRIR_{225}$ is less susceptible to anomalous fading, and so involves a smaller fading correction. Measuring both signals gives the option of using either, or both, for burial-dose estimation. However, accuracy of the IR_{50} D_e may be compromised when the signal is measured in a post-IR protocol, and this is suggested by the imperfect dose-recovery results obtained (Fig. 3). Nevertheless, those clasts that showed a good burial-dose profile for both signals also gave consistent burial dose estimates from the two signals (Table 1; Fig. 6); it may be that the inaccuracy in laboratory dose recovery is less important for recovering natural doses.

Profiles were fitted using the simplest available model for luminescence depth profiles (one bleach, one burial). For some cores a more complex model may be justified, but our interest here is the inferred signal at the surface, which would not be greatly affected by a more complex model. Processing was done using a Bayesian fitting routine, with the derived estimate of the natural luminescence signal at the surface, L_B, used directly in the dose-response function. With this routine, an estimate of L_B is obtained even if the surface is not fully bleached. For example, clast T5-7-A1 (Fig. 5) shows a burial dose plateau for the IR_{50} signal, but no such plateau for the $pIRIR_{225}$. The fitting routine provides an estimate of L_B for both signals, albeit a very imprecise estimate for in the case of the $pIRIR_{225}$. In principle there is still value in the imprecise L_B, when considered with other information: in Fig. 6, the imprecise $pIRIR_{225}$ L_B is converted to an age estimate in the range of 0–10 ka, which is consistent with the more precise IR_{50} age for the same core. In practice, however, the extra (imprecise) information has not proven useful for the sites considered here. Furthermore, there is a concern over data integrity in the absence of a burial-dose plateau. The presence of a plateau indicates not just that a sample was fully bleached before burial, but also that the sample has not been bleached *since* burial, i.e. through a recent period of exposure. A failure to identify reworking of this sort may account for the anomalously young ages of location T4 at Site 1.

The consistency in the age estimates at Site 1 (T5, T6, T7) also indicates that the innovative dose rate methodology is performing well. The dose rates within these locations ranges from 4.5 to 9 Gy ka^{-1}, so the consistent ages for the samples imply that the dose rates a correctly accounting for the variation in D_e. The dose rate measurements rely on very small sample sizes: only a few grams are used in the preparation of beta-counter samples, and a little more added to define the relative activities using gamma spectrometry. Small sample sizes are sufficient because of the relatively high activity of the granite clasts, and because of the high counting efficiency, and low background, of the beta-counting instrument. Small sample sizes (single cores) are also sufficient for measurement of luminescence profiles and equivalent dose, although with a possible reduction in precision of D_e. By using smaller samples, a larger number of clasts can be measured, increasing the chances of finding well-bleached and dateable clasts. However, this presents a practical problem of sampling, because a large number of clasts must be transported from the field to the laboratory for coring. A solution to the transport problem would be *on-site* drilling of cores: a technical challenge, but not an insurmountable one, and it should be addressed in future work to enable a better exploitation of rock surface luminescence dating.

5. Conclusion

Mass-transport deposits are potentially dateable using rock-surface burial methods. It is shown here that reproducible ages can be obtained for cobble clasts extracted from colluvial and debris-flow sediment. Nevertheless, it is unlikely that all clasts received sufficient daylight exposure before burial to reset the surface luminescence signal. The major challenge, therefore, is in collecting and measuring sufficient number of clasts for enough confidence in the ages produced. We altered the normal measurement strategy to increase the number of clasts measured, with a small and acceptable cost in measurement precision. Adaptations were made to measurement procedures to determine the equivalent dose, and the dose rate, using less material and fewer measurements per dated clast than normally required.

For the Caucasus region investigated here, hillslope colluvium was found to be extremely suitable for rock-surface burial dating– prolonged exposure on the hillslope means that the luminescence signal at the cobble surface is usually well-bleached before burial. Consistent burial ages of 6–8 ka have been determined for this site, correspond to a wetter climatic phase in the Caucasus during the early-to-mid Holocene. The quality of pre-burial bleaching is more mixed in the case of debris-flow clasts. Nevertheless, the residual dose of modern debris-flow casts is reasonable low– equivalent to 1–2 ka. Two clasts extracted from a debris-flow unit of the Tyubele swell returned ages in the range of 10–20 ka; while imprecise, the ages are consistent with a late-glacial formation age of this enigmatic feature.

Declaration of competing interest

None.

Acknowledgments

Funding provided by the Independent Research Fund Denmark – Natural Sciences, grant number 6108-00532B. R. Kurbanov was supported by Russian Science Foundation (19-77-10077), D. Semikolennykh acknowledges the Institute of Geography RAS (state program 0148-2019-0005), D. Khashchevskaya was supported by Lomonosov MSU (state program 121051100135-0).

References

al Khasawneh, S., Murray, A., Thomsen, K., AbuAzizeh, W., Tarawneh, M., 2019. Dating a near eastern desert hunting trap (kite) using rock surface luminescence dating. Archaeol. Anthropol. Sci. 11, 2109–2119. https://doi.org/10.1007/s12520-018-0661-3.

Ankjærgaard, C., Murray, A.S., 2007. Total beta and gamma dose rates in trapped charge dating based on beta counting. Radiat. Meas. 42, 352–359. https://doi.org/10.1016/j.radmeas.2006.12.007.

Auclair, M., Lamothe, M., Huot, S., 2003. Measurement of anomalous fading for feldspar IRSL using SAR. Radiat. Meas. 37, 487–492. https://doi.org/10.1016/S1350-4487(03)00018-0.

Bashenina, N., Tushinsky, G., Golubev, G., Myagkov, S., 1974. Brief Outline of the Elbrus Region Geomorphology (In Russian) [геоМорфологический Очерк Приэльбрусья]. Moscow State University, Moscow.

Buylaert, J.-P., Jain, M., Murray, A.S., Thomsen, K.J., Thiel, C., Sohbati, R., 2012. A robust feldspar luminescence dating method for Middle and Late Pleistocene sediments. Boreas 41, 435–451. https://doi.org/10.1111/j.1502-3885.2012.00248.x.

Carpenter, B., Gelman, A., Hoffman, M.D., Lee, D., Goodrich, B., Betancourt, M., Brubaker, M., Guo, J., Li, P., Riddell, A., 2017. Stan: a probabilistic programming language. J. Stat. Software 76.
Connor, S.E., Kvavadze, E.V., 2009. Modelling late Quaternary changes in plant distribution, vegetation and climate using pollen data from Georgia, Caucasus. J. Biogeogr. 36, 529–545.
Cunningham, A.C., Murray, A.S., Armitage, S.J., Autzen, M., 2018. High-precision natural dose rate estimates through beta counting. Radiat. Meas. 120, 209–214. https://doi.org/10.1016/j.radmeas.2018.04.008.
Freiesleben, T., Sohbati, R., Murray, A., Jain, M., al Khasawneh, S., Hvidt, S., Jakobsen, B., 2015. Mathematical model quantifies multiple daylight exposure and burial events for rock surfaces using luminescence dating. Radiat. Meas. 81, 16–22. https://doi.org/10.1016/j.radmeas.2015.02.004.
Fuchs, M., 2019. Applications in fluvial and hillslope environments. In: Bateman (Ed.), Handbook of Luminescence Dating. Whittles, Dunbeath.
Galbraith, R.F., Roberts, R.G., Laslett, G.M., Yoshida, H., Olley, J.M., 1999. Optical dating of single and multiple grains of quartz from Jinmium rock shelter, northern Australia: Part I, experimental design and statistical models. Archaeometry 41, 339–364.
Gelman, A., Rubin, D.B., 1992. Inference from iterative simulation using multiple sequences. Stat. Sci. 7, 457–472.
Gobejishvili, R., Lomidze, N., Tielidze, L., 2011. Chapter 12 - late Pleistocene (Würmian) glaciations of the Caucasus. In: Ehlers, J., Gibbard, P.L., Hughes, P.D. (Eds.), Developments in Quaternary Sciences, Quaternary Glaciations - Extent and Chronology. Elsevier, pp. 141–147. https://doi.org/10.1016/B978-0-444-53447-7.00012-X.
Grachev, A.M., Novenko, E.Y., Grabenko, E.A., Alexandrin, M.Y., Zazovskaya, E.P., Konstantinov, E.A., Shishkov, V.A., Lazukova, L.I., Chepurnaya, A.A., Kuderina, T. M., 2020. The Holocene Paleoenvironmental History of Western Caucasus (Russia) Reconstructed by Multi-Proxy Analysis of the Continuous Sediment Sequence from Lake Khuko. The Holocene 0959683620972782.
Greilich, S., Glasmacher, U.A., Wagner, G.A., 2005. Optical dating of granitic stone surfaces. Archaeometry 47, 645–665. https://doi.org/10.1111/j.1475-4754.2005.00224.x.
Guérin, G., Mercier, N., Adamiec, G., 2011. Dose-rate conversion factors: update. Ancient TL 29, 5–8.
Guérin, G., Mercier, N., Nathan, R., Adamiec, G., Lefrais, Y., 2012. On the use of the infinite matrix assumption and associated concepts: a critical review. Radiat. Meas. 47, 778–785. https://doi.org/10.1016/j.radmeas.2012.04.004.
Hansen, V., Murray, A., Thomsen, K., Jain, M., Autzen, M., Buylaert, J.-P., 2018. Towards the origins of over-dispersion in beta source calibration. Radiat. Meas. 120, 157–162. https://doi.org/10.1016/j.radmeas.2018.05.014.
Huntley, D.J., Lamothe, M., 2001. Ubiquity of anomalous fading in K-feldspars and the measurement and correction for it in optical dating. Can. J. Earth Sci. 38, 1093–1106. https://doi.org/10.1139/e01-013.
Jenkins, G.T.H., Duller, G.A.T., Roberts, H.M., Chiverrell, R.C., Glasser, N.F., 2018. A new approach for luminescence dating glaciofluvial deposits - high precision optical dating of cobbles. Quat. Sci. Rev. 192, 263–273. https://doi.org/10.1016/j.quascirev.2018.05.036.
Joannin, S., Ali, A.A., Ollivier, V., Roiron, P., Peyron, O., Chevaux, S., Nahapetyan, S., Tozalakyan, P., Karakhanyan, A., Chataigner, C., 2014. Vegetation, fire and climate history of the Lesser Caucasus: a new Holocene record from Zarishat fen (A rmenia). J. Quat. Sci. 29, 70–82.
King, G., Valla, P.G., Lehmann, B., 2019. Rock surface burial and exposure dating. In: Bateman (Ed.), Handbook of Luminescence Dating. Whittles, Dunbeath.
Knyazev, A.V., Savinetskiy, A.B., Gei, N.A., 1992. The History of the Vegetation Cover of North Ossetia in the Holocene (in Russian). Nauka, Moscow.
Koronovskiy, N.V., Milanovskiy, E.E., 1960. The Origin of the Tubele Hill in the Baksan Valley (Central Caucasus) (In Russian) [ПроисхоЖдение Вала Тюбеле В Ущелье Баксана (Центральный Кавказ)]. Vestnik MGU [bulletin of Moscow State University. Geology series 69–77.
Liu, J., Cui, F., Murray, A.S., Sohbati, R., Jain, M., Gao, H., Li, W., Li, C., Li, P., Zhou, T., Chen, J., 2019. Resetting of the luminescence signal in modern riverbed cobbles along the course of the Shiyang River, China. Quat. Geochronol. 49, 184–190. https://doi.org/10.1016/j.quageo.2018.04.004.
Meyer, M.C., Gliganic, L.A., Jain, M., Sohbati, R., Schmidmair, D., 2018. Lithological controls on light penetration into rock surfaces – implications for OSL and IRSL surface exposure dating. Radiat. Meas. 120, 298–304. https://doi.org/10.1016/j.radmeas.2018.03.004.
Murray, A., Marten, R., Johnston, A., Martin, P., 1987. Analysis for naturally occurring radionuclides at environmental concentrations by gamma spectrometry. J. Radioanal. Nucl. Chem. 115, 263–288. https://doi.org/10.1007/bf02037443.
Murray, A.S., Helsted, L.M., Autzen, M., Jain, M., Buylaert, J.P., 2018. Measurement of natural radioactivity: calibration and performance of a high-resolution gamma spectrometry facility. Radiat. Meas. 120, 215–220. https://doi.org/10.1016/j.radmeas.2018.04.006.
Ou, X.J., Roberts, H.M., Duller, G.A.T., Gunn, M.D., Perkins, W.T., 2018. Attenuation of light in different rock types and implications for rock surface luminescence dating. Radiat. Meas. 120, 305–311. https://doi.org/10.1016/j.radmeas.2018.06.027.
Rades, E.F., Sohbati, R., Lüthgens, C., Jain, M., Murray, A.S., 2018. First luminescence-depth profiles from boulders from moraine deposits: insights into glaciation chronology and transport dynamics in Malta valley, Austria. Radiat. Meas. 120, 281–289. https://doi.org/10.1016/j.radmeas.2018.08.011.
Riedesel, S., Autzen, M., 2020. Beta and gamma dose rate attenuation in rocks and sediment. Radiat. Meas. 133, 106295. https://doi.org/10.1016/j.radmeas.2020.106295.
Seinova, I.B., Sidorova, T.L., Chernomorets, S.S., 2007. Processes of debris flow formation and the dynamics of glaciers in the Central Caucasus. In: Debris-flow Hazards Mitigation: Mechanics, Prediction, and Assessment. Millpress, Rotterdam, pp. 77–85.
Serebryanniy, L.R., Golodkovskaya, N.A., Orlov, A.V., Maljasova, E.S., Ilves, E.O., 1984. Glacier Fluctuations and Moraine Accumulation Processes in the High Mountain Caucasus (Kolebanija Lednikov I Processy Morenonakoplenija Na Vysokogornom Kavkaze). Nauka, Moskow.
Shcherbakova, E., 1973. Ancient Glaciation of the Greater Caucasus. (In Russian) [Древнее Оледенение Большого Кавказа]. Moscow State University.
Simms, A.R., DeWitt, R., Kouremenos, P., Drewry, A.M., 2011. A new approach to reconstructing sea levels in Antarctica using optically stimulated luminescence of cobble surfaces. Quat. Geochronol. 6, 50–60. https://doi.org/10.1016/j.quageo.2010.06.004.
Sohbati, R., Jain, M., Murray, A., 2012. Surface exposure dating of non-terrestrial bodies using optically stimulated luminescence: a new method. Icarus 221, 160–166. https://doi.org/10.1016/j.icarus.2012.07.017.
Sohbati, R., Murray, A., Jain, M., Buylaert, J.-P., Thomsen, K., 2011. Investigating the resetting of OSL signals in rock surfaces. Geochronometria 38, 249–258. https://doi.org/10.2478/s13386-011-0029-2.
Sohbati, R., Murray, A.S., Porat, N., Jain, M., Avner, U., 2015. Age of a prehistoric "Rodedian" cult site constrained by sediment and rock surface luminescence dating techniques. Quat. Geochronol. 30, 90–99. https://doi.org/10.1016/j.quageo.2015.09.002.
Solomina, O.N., Bradley, R.S., Hodgson, D.A., Ivy-Ochs, S., Jomelli, V., Mackintosh, A.N., Nesje, A., Owen, L.A., Wanner, H., Wiles, G.C., Young, N.E., 2015. Holocene glacier fluctuations. Quat. Sci. Rev. 111, 9–34. https://doi.org/10.1016/j.quascirev.2014.11.018.
Souza, P.E., Sohbati, R., Murray, A.S., Clemmensen, L.B., Kroon, A., Nielsen, L., 2021. Optical dating of cobble surfaces determines the chronology of Holocene beach ridges in Greenland. Boreas n/a. https://doi.org/10.1111/bor.12507.
Souza, P.E., Sohbati, R., Murray, A.S., Kroon, A., Clemmensen, L.B., Hede, M.U., Nielsen, L., 2019. Luminescence dating of buried cobble surfaces from sandy beach ridges: a case study from Denmark. Boreas 48, 841–855. https://doi.org/10.1111/bor.12402.
Tamura, T., Cunningham, A.C., Oliver, T.S.N., 2019. Two-dimensional chronostratigraphic modelling of OSL ages from recent beach-ridge deposits, SE Australia. Quat. Geochronol. 49, 39–44. https://doi.org/10.1016/j.quageo.2018.03.003.
Tanner, A.B., 1980. Radon Migration in the Ground: a Supplementary Review.
Tarbeeva, A.M., 2008. Guide to the Field Trip of the International Conference "Debris Flows: Disasters. Risk, Forecast, Protection.
Vafiadou, A., Murray, A.S., Liritzis, I., 2007. Optically stimulated luminescence (OSL) dating investigations of rock and underlying soil from three case studies. J. Archaeol. Sci. 34, 1659–1669. https://doi.org/10.1016/j.jas.2006.12.004.

Further reading

Bertolini, G., 2007. Radiocarbon dating on landslides in the northern Apennines (Italy), in: landslides and climate change: challenges and solutions. In: Mathie, E., McInnes, R., Fairbank, H., Jakeways, J. (Eds.), Proceedings of the International Conference on Landslides and Climate Change, Ventnor. Taylor & Francis, pp. 73–80.
Chapot, M.S., Sohbati, R., Murray, A.S., Pederson, J.L., Rittenour, T.M., 2012. Constraining the age of rock art by dating a rockfall event using sediment and rock-surface luminescence dating techniques. Quat. Geochronol. 13, 18–25. https://doi.org/10.1016/j.quageo.2012.08.005.
McCarroll, D., Shakesby, R.A., Matthews, J.A., 2001. Enhanced rockfall activity during the Little Ice Age: further lichenometric evidence from a Norwegian talus. Permafr. Periglac. Process. 12, 157–164. https://doi.org/10.1002/ppp.359.
Seynova, I.B., Popovnin, V.V., Zolotaryov, Y.A., 2003. Intensification of glacial debris flows in the Gerkhozhan River basin, Caucasus, in the late 20th century. Landslide News 14, 39–43.
Stoffel, M., 2006. A review of studies dealing with tree rings and rockfall activity: the role of dendrogeomorphology in natural hazard Research. Nat. Hazards 39, 51–70. https://doi.org/10.1007/s11069-005-2961-z.